Scaling of shear–generated turbulence: the equatorial thermocline, a case study

K. J. Richards,[1,2] A. Natarov,[1] G. S. Carter,[2]

K. J. Richards, International Pacific Research Center, University of Hawai'i at Mānoa, 1680 East West Road, Honolulu, HI 96822, USA. (rkelvin@hawaii.edu)

A. Natarov, International Pacific Research Center, University of Hawai'i at Mānoa, 1680 East West Road, Honolulu, HI 96822, USA. (natarov@hawaii.edu)

G. S. Carter, Department of Oceanography, University of Hawai'i at Mānoa, 1000 Pope Road, Honolulu, HI 96822, USA. (gscarter@hawaii.edu)

[1]International Pacific Research Center,
University of Hawai'i at Mānoa, Honolulu,
Hawai'i, USA.

[2]Department of Oceanography, University
of Hawai'i at Mānoa, Honolulu, Hawai'i,
USA.

Abstract. We formulate an expression for the turbulent kinetic energy dissipation rate, ϵ, associated with shear–generated turbulence in terms of readily measured properties of the flow or easily derived quantities in models. The expression depends on the turbulent vertical length scale, ℓ_v, the inverse time scale N and the Richardson number $Ri = N^2/S^2$, where S is the vertical shear, with ℓ_v scaled in a way consistent with theories and observations of stratified turbulence. Unlike previous studies the focus is not so much on the functional form of Ri, but the vertical variation of the length scale ℓ_v. Using data from two $\sim$7 day time series in the western equatorial Pacific the scaling is compared with the observed ϵ. The scaling works well with the estimated ϵ capturing the differences in amplitude and vertical distribution of the observed ϵ between the two times series. Much of those differences are attributable to changes in the vertical distribution of the length scale ℓ_v, and in particular the associated turbulent velocity scale, u_t. We relate u_t to a measure of the fine-scale variations in velocity, $\tilde{u}$. Our study highlights the need to consider the length scale and its estimation in environmental flows. The implications for the vertical variation of the associated turbulent diffusivity are discussed.

1. Introduction

Shear–generated turbulence in stably stratified environmental flows often makes an important contribution to the vertical transport of properties. Because of this, there have been numerous studies to develop parameterization schemes that provide an estimate of these turbulent fluxes with varying degrees of sophistication. Here we consider the scaling of the turbulent kinetic dissipation rate, ϵ, a measure of turbulent activity. The scaling is put in terms of readily measured properties of the flow or easily derived quantities in models. As such the scaling can form the basis of a parameterization scheme to estimate turbulent fluxes from observations and be included in models of the ocean and atmosphere.

A large number of schemes relate the turbulent activity to the local gradient Richardson number, $Ri = N^2/S^2$, where N and S are the buoyancy frequency and vertical shear, respectively. In doing so, it is important that both N and the turbulence generating shear S are adequately resolved, something which is not always the case in the application of such schemes [c.f. *Richards et al.*, 2015]. Much of the focus has been on the functional form of the Richardson number; see e.g. *Pacanowski and Philander* [1981], *Peters et al.* [1988], and Figure 1 of *Zaron and Moum* [2009]. As pointed out by *Zaron and Moum* [2009], however, the turbulent properties also depend on an appropriate length and time scale. Our focus will be on the turbulent vertical length scale, ℓ_v, its vertical variation and its impact on the vertical variation of the turbulent kinetic energy dissipation rate, ϵ, and associated vertical diffusion coefficient, κ_v.

In this study we formulate an expression for ϵ that depends on the length scale, ℓ_v, the inverse time scale N and the Richardson number Ri. Using a similar expression,

and observations from the western equatorial Pacific with both S and N well resolved, *Richards et al.* [2015] find the implied length scale ℓ_v is consistent with studies on stratified turbulence. We extend their work by consideration of the vertical variation of ℓ_v, and in particular the associated turbulent velocity scale, u_t, , and how to relate it to readily measured quantities or easily derived quantities in models. The scaling is compared to additional measurements of ϵ in the western equatorial Pacific. The comparison is very encouraging and highlights the importance of the vertical variation of the turbulent velocity scale.

2. Data and physical setting

Data were collected from cruise KM1208 of the R/V Kilo Moana to the western equatorial Pacific in April/May 2012. Here we consider data taken on a meridional transect along 156°E from 5°N to 1°S, during April 20-24, with stations at half degree intervals together with two time series. The two time series were conducted at the equator (nominally) and 1.375N, 156°E, for 8 and 7 days respectively. For the first 3 days of the equatorial time series the ship performed a butterfly pattern of side half a degree (∼50km). The variation of properties on this scale was found to be small so the remainder of the time series was conducted from a stationary ship at the equator.

The combination of instruments used was similar to that described in *Richards et al.* [2015] with the exception that an untethered microstructure probe was used. High vertical resolution velocity data were collected using a 600 kHz Teledyne RDI Workhorse Acoustic Doppler Current Profiler attached to a CTD frame and operated in lowered mode (LADCP). CTD/LADCP profiles were taken at a nominal 2 hour interval to a depth of 500m during the two time series. Turbulence measurements were taken during the two

time series using a (untethered) Rockland VMP 6000 fitted with two shear probes, and two rapid temperature probe (FP07). A total of 24 and 25 profiles were taken during the equatorial and 1.375°N time series, respectively, at irregular intervals but spanning the duration of each time series. All VMP profiles were deeper than 500m with most being full depth (∼1940m and ∼2400m at the two sites, respectively).

The LADCP and VMP data were processed in the same way as described in *Richards et al.* [2015]. In particular, the LADCP velocity data were binned at 2m depth intervals while the turbulent kinetic energy dissipation rate, ϵ, calculated from the microstructure shear measurements, was averaged over 1m. As shown by *Richards et al.* [2015] the relatively high vertical resolution, particularly the LADCP velocity, is needed to capture the finescale flow features that generate the turbulence.

The eastward (zonal) component of velocity, u, along the meridional section is shown in Figure 1a. Also plotted are contours of potential density and the mixed layer depth. The latter is determined as the depth at which the potential density first exceeds the surface density by $\Delta\sigma = 0.02$ kg m^{-3} (a value that captures well the depth to which surface induced turbulence penetrates). The mixed layer depth is in general shallower than 50m except towards the northern extreme of the section.

At this time and longitude the equatorial undercurrent (EUC) is centered at a depth of around 220m and displaced south of the equator. The north equatorial counter current (NECC) is centered at 2.5°N and 120m depth. At the surface close to the equator the eastward flowing current is a result of a westerly wind event that occurred just prior to the section being made.

The positioning of both the EUC and NECC is such that the lateral shear is conducive to inertial instability [*Richards and Edwards*, 2003; *Natarov and Richards*, 2015]. The along isopycnal value of fQ averaged between isopycnals with mean depth 100-120m and 180-200m is shown in Figures 1b and c, respectively, where f is the Coriolis parameter and Q is the potential vorticity approximated by $(f - \partial u/\partial y)N^2$, i.e. assuming $\partial u/\partial y \gg \partial v/\partial x$ and the hydrostatic approximation [*Vallis*, 2006], with u and v the components of velocity in the zonal and meridional directions (x, y), respectively, and N the buoyancy frequency. For comparison, the thin lines in Figures 1b and c are the background $fQ = f^2 N_0^2$, where N_0^2 is the average N^2 along the layers. The depth averaged fQ between 180-200m is negative between 0.5°S and 0.4°N, a necessary condition for inertial instability, while between 100-120m fQ is close to zero from the equator to 2°N, consistent with the mature phase of the instability [*Natarov and Richards*, 2015].

The vertical shear of the meridional component of velocity, $\partial v/\partial z$, and buoyancy frequency, N, are shown in Figure 2 for the two time series. (The few cases of $N^2 < 0$ are set to zero.) The quantities are plotted on potential density surfaces mapped back to the mean depth of each surface. Both quantities are seen to have features that have a relatively small vertical scale that are persistent in time (particularly at the equator). We will refer to such features as SVS (small vertical scale) features. The SVS features have a somewhat different character at the equator and 1.375°N. At the equator the higher amplitude SVS features are distributed between 100-250m depth, while at 1.375°N they are concentrated around 175m.

The variance preserving spectra of the zonal and meridional components of vertical shear, $\partial u/\partial z$ and $\partial v/\partial z$, respectively, where z is the vertical coordinate, (Fig. 3), have

peaks at around 25-40m wavelength. It is noteworthy that the peak in the shear spectrum for v is higher than that for u in this wavenumber band, particularly at the equator. Similar examples are shown in *Richards et al.* [2015].

The time mean turbulent kinetic energy dissipation rate, ϵ, from the two time series is shown in Figure 4 (red lines) as a function of depth over the depth range 50-350m. Both show elevated ϵ below 100m, with ϵ at 1.375°N reaching somewhat greater values. The vertical distributions of the elevated ϵ reflect, to some extent, the different vertical distribution of SVS features at the two locations.

The full depth range profiles of time mean ϵ are shown in Figure 5. There are patches of elevated mean ϵ below the thermocline at each location, particular between 500-1000m depth at 1.375°N and an increase towards the bottom at the equator.

3. Scaling of shear–generated turbulence

We start by writing the turbulent kinetic energy dissipation rate, ϵ, as

$$\epsilon = \ell_v^2 N^3 f(Ri) \tag{1}$$

[see e.g. *Richards et al.*, 2015] where ℓ_v is a turbulent length scale and $f(Ri)$ is a function of the Richardson number, $Ri = N^2/S^2$, with S being the vertical shear.

The length scale ℓ_v can be written as

$$\ell_v = c\frac{u_t}{N} \tag{2}$$

where u_t is a velocity scale. Taking u_t to be the horizontal velocity scale of the turbulent flow then this scaling has been found in a number of studies on stratified turbulent flows

with ℓ_v being the vertical scale of the turbulent flow, when the flow is in the strong turbulence limit given when the buoyancy Reynolds number $\mathcal{R} = \epsilon/(\nu N^2) \gg 1$, where ν is the kinematic viscosity of the fluid (e.g. *Godeferd and Staquet* [2003], *Waite and Bartello* [2004], *Brethouwer et al.* [2007], *Bartello and Tobias* [2013]). The measurements used here indicate the turbulence is in the strong regime. We have introduced a non-dimensional constant c which will be determined by fitting (1) to observations.

To express u_t in terms of an observable quantity we assume $u_t \simeq 0.1\tilde{u}$ where $\tilde{u}$ is a measure of the amplitude of the SVS flow features. The factor 0.1 is based on experimental and DNS studies and is expected to be a rough upper bound with substantially smaller values as the turbulence grows and decays (see e.g. Figure 12 of *Koop and Browand* [1979]; Figures 2 and 3 of *Smyth et al.* [2005]). The constant c in (2) accounts for departures from $u_t = 0.1\tilde{u}$ in the time mean and the way $\tilde{u}$ is determined.

Based on measurements from multiple cruises to the western equatorial Pacific *Richards et al.* [2015] find $\epsilon \sim N$ at constant Richardson number, which implies $\ell_v \sim 1/N$. They argue this is equivalent to (2) by noting the depth average value of $\tilde{u}$ (and hence u_t) was approximately constant between the data sets considered.

Here we will consider $\tilde{u}$ in more detail. In particular, given the differences in the vertical distribution of SVS features in Figure (2) we will consider the vertical distribution of $\tilde{u}$. For each profile of u and v we apply a wavelet transform (using a Morlet wavelet), average the local wavelet power spectrum between 10-50m wavelength, and normalize so that the depth average variance between 50-250m is equal to the variance of the original profile (after a high-pass Fourier filter has been applied with a cutoff of 100m to capture the peak in the shear spectrum). The SVS velocity scale $\tilde{u}$ is then taken as the root mean square of

the individual profiles from u and v. The result, averaged over each time series, is shown in Figure 6 as a function of depth at the equator and 1.375°N. The vertical profiles of $\tilde{u}$ at the two sites are different. At the equator the mean $\tilde{u}$ is elevated over a relatively broad depth range between 100m to 200m with a maximum of approximately 0.08 ms^{-1}. In contrast the profile at 1.375°N is more peaked at a depth of 180m with a maximum values of 0.12 ms^{-1}. The SVS velocity scale, $\tilde{u}$ drops off with depth for both time series to a value of approximately 0.03ms^{-1} at 350m depth. The vertical variation of $\tilde{u}$ puts into question the assumption of *Richards et al.* [2015] that it is essentially independent of N when considering the form of the vertical scale ℓ_v. We will return this point.

Lastly, $f(Ri)$ needs to be specified. We will take

$$f(Ri) = e^{-bRi} \tag{3}$$

for Ri<0.25. Fitting (1) to the distribution found by *Richards et al.* [2015] (their Fig. 6) we obtain b=4.81. For Ri>0.25 f is ramped down to 0 at Ri=0.5 and remains zero for higher values of Ri. Note there is only a modest increase in f as Ri tends to zero; Ri increases only by a factor of 3 from Ri=0.25 to Ri=0. This is in contrast to some other formulations such as that of *Kunze et al.* [1990] (see Fig. 6, *Richards et al.* 2015). We will discuss the sensitivity to our choices in the next section but note here that the vertical distribution of ϵ as prescribed by (1) is much more dependent on the vertical distribution of ℓ_v through variations in $\tilde{u}$ than the functional form of f.

4. Comparison with observations

The scaling described above involves relating the turbulent kinetic energy dissipation rate, ϵ, to the turbulent length scale, ℓ_v, the buoyancy frequency, N, and a function of the Richardson number $f(Ri)$: equations (1), (2) and (3). In addition we relate the turbulent velocity scale, u_t, to the SVS velocity scale $\tilde{u}$, by $u_t = 0.1\tilde{u}$.

To evaluate the scheme we utilize the two time series at the equator and 1.375°N each of which have around 90 vertical profiles of velocity and density. The vertical shear, S, has a nominal vertical resolution of 2m, while N is calculated from 1 decibar (∼1m) averages of salinity and temperature. Data are interpolated onto a common vertical grid and ϵ calculated using (1). The SVS velocity scale, $\tilde{u}$ is calculated for each profile as outlined above. The resultant estimate for ϵ is then averaged over all profiles for each time series. The result is shown in Figure 4 for each time series (blue lines) and compared to the observed averaged profiles (red lines).

The constant c in (2) is taken to be $c = 0.24$, which is the mean value of c for each time series got by fitting the estimated ϵ to the observed over the depth interval 100-250m (c estimated in this way for each time series is 0.23 and 0.25, respectively). Given that our use of $u_t = 0.1\tilde{u}$ is an upper bound on u_t, the value of c (and its small variation between time series) suggests the scalings used are appropriate.

The estimated ϵ compares remarkably well for both time series over the depth interval 50-350m. In particular, the change in vertical distribution and amplitude are captured well. It is stressed that much of the vertical variation in the estimated ϵ is controlled by the vertical variation in the estimated vertical scale ℓ_v through the assumed dependence on $\tilde{u}$ (compare Figure 4 with Figure 6). The SVS velocity scale, $\tilde{u}$, is only modestly sensitive to

our choices in how $\tilde{u}$ is computed. For instance, the 50m cutoff for the wavelet spectrum was chosen to limit end effects (the cone-of-influence). Increasing this to 100m gives a slightly degraded (visual) fit over the full depth, with the fitted value of c increased slightly by 5%.

The turbulent kinetic energy dissipation rate, ϵ, estimated from (1), bin averaged with respect to $\log_{10}S^2$ and $\log_{10}N^2$, together with the number of occurrences in each bin average are shown in Figure 7 for the equatorial time series for data between depths 50-250m. The distributions are very similar to those shown in Figs. 4a and b *Richards et al.* [2015] showing an increase in ϵ at constant Richardson number for increasing N^2 (equivalently, increasing S^2) and the peak in the number of occurrences between Ri=0.25 and 5.

The vertical variation of the time mean of the turbulent length scale, ℓ_v, given by 2 is shown in Figure 8 for the two time series. At the equator, overall there is a slight decrease of ℓ_v with depth to a value of approximately 0.2m at 300m depth followed by an increase. At 1.375°N, between 50-150m, ℓ_v is somewhat larger than at the equator with a value around 0.4m. There is a sharp decrease at 150m with ℓ_v reducing to around 0.2m. Again there is an increase in ℓ_v at deeper depths, in this case starting around 250m depth.

The time mean turbulent length scale, ℓ_v, is compared to the time mean Osmidov scale $\ell_o = \sqrt{\epsilon/N^3}$ in Figure 8. The vertical variation of the two length scales is very similar in both time series. Between 175-275m they are very similar in magnitude. Between 50-150m, ℓ_o is greater than ℓ_v by a factor of approximately 1.5 on average in both cases.

Given the vertical distribution of $\tilde{u}$ and a possible dependence on N we revisit the relationship between ϵ and N at constant Ri. Similar to *Richards et al.* [2015] we calculate

the average, in our case, estimated ϵ in a band of Ri of width 0.1 centered on Ri=0.25 for varying N^2. We find $\epsilon \sim N^{-1.28\pm0.05}$. The negative slope is somewhat greater than 1, indicating that a dependency of $\tilde{u}$ on N feeds through to the mean characteristics of the average ϵ at constant Ri, but not overly so. *Richards et al.* [2015] found $\epsilon \sim N^{-1.07\pm0.18}$. There is a slight overlap in the 95% confidence limits, but differences in the slope may occur because of differences in the flow regime and stratification, something that requires further study.

5. Deconstruction of the scaling

Combining (1) and (2), and relating the turbulent velocity scale u_t to the SVS velocity scale $\tilde{u}$, gives

$$\epsilon \sim \tilde{u}^2 N f(Ri) \tag{4}$$

To determine which factor most influences the vertical distribution of ϵ we plot the time mean of each term on the right-hand side of (4) separately in Figures 9 and 10 a-c for the equatorial and 1.375°N time series, respectively. Each term has been normalized with its depth mean to emphasize the depth variation. The fourth panel (d) in each Figure shows the time mean of ϵ estimated from (4). Here ϵ has been normalized with its value averaged between 250-300m depth. Also shown in panel (d) is the product of the time mean of the 3 terms on the right-hand side of (4), normalized in the same way (thin dashed blue line), which captures much of the vertical variation of the time mean of ϵ.

Also shown in Figures 9d and 10d is ϵ estimated by (4) but with $\tilde{u}$ held constant (i.e. $\epsilon \sim N f(Ri)$: red line in the figures). Again the estimate of ϵ has been normalized by its

value averaged between 250-300m. The vertical variation in ϵ is reduced substantially at both locations compared with when the full expression (4) is used. Much of the vertical variation in N is compensated by the variation in $f(Ri)$. The vertical variation in ϵ is very much reflected in the variations in $\tilde{u}^2$; compare Figures 9a and d, and Figures 10a and d.

To test the sensitivity to the choice of $f(Ri)$, in Figures 9c and 10c we compare the time mean normalized vertical variation of our choice of $f(Ri)$ with the functional form, $f_k(Ri)$, suggested by *Kunze et al.* [1990]. Their expression for ϵ can be written $\epsilon_k \sim \Delta z N^3 f_k(Ri)$, where Δz is the thickness of a layer where $Ri < Ri_{cr}$ and Ri_{cr} is critical Richardson number taken here to be 0.5 to be consistent with our choice of when $f(Ri)$ becomes zero (Eq. 6 of [*Richards et al.*, 2015]). The vertical variation of the time mean $f(Ri)$ and $f_k(Ri)$ is very similar at both locations despite their very different behavior at small Ri ($f_k(Ri) \sim 1/Ri^{3/2}$ for $Ri \ll Ri_{cr}$). The reason for this similarity is the distribution of data in (N^2,S^2) space is confined and centered on Ri between 0.25 and 0.5 (Fig. 7b). (Note, the scaling ϵ_k is similar to (4) if $\Delta z \sim \tilde{u}/N$ which is explored by *Richards et al.* [2015].)

6. Vertical distribution of the vertical diffusion coefficient

Combining (1) and (2), the vertical turbulent diffusion coefficient, κ_v ($= \gamma\epsilon/N^2$) [*Osborn*, 1982] becomes

$$\kappa_v = \frac{c\gamma u_t^2 f(Ri)}{N}. \tag{5}$$

where we take $u_t = 0.1\tilde{u}$ and $c = 0.24$. We will take the mixing efficiency $\gamma = 0.2$, recognizing the uncertainties in the value of γ and expected spatial and temporal variations. *Ijichi and Hibiya* [2018] find a tendency for γ to increase with depth as the stratification weakens, but in depths less than 500m the spread of values of γ is approximately centered on 0.2. Here we are interested in how the scaling of ϵ given in (4) translates to κ_v.

The time mean κ_v estimated by (5) is shown in Figures 11a and b (blue lines) for the equator and 1.375°N time series, respectively. The factor N^{-2} reshapes the vertical profile of κ_v compared to ϵ (see Figs. 9d and 10d, respectively) such that κ_v is reduced in the pycnocline at around 200m depth for the 1.375°N time series where $\tilde{u}$ and ϵ peak, and the maximum value of κ_v occurs at a somewhat shallower depth. The depth averaged κ_v between 50-170m for the 1.375°N time series (4.6×10^{-5} m^{2}s^{-1}), is more than twice that at the equator (2.0×10^{-5} m^{2}s^{-1}). Below the pycnocline, the reduced SVS activity (reduced $\tilde{u}$) tends to compensate the reduced stratification such that we do not see a marked increase in κ_v.

The vertical variation in κ_v is dependent on the combination of the vertical variations of Ri, $\tilde{u}$ and N. To compare with a scheme that considers only the first of these, the Richardson number, in Figures 11a and b (red lines) we show the results using the KPP scheme of *Large et al.* [1994] for shear–generated turbulence, namely

$$\kappa_{KPP} = \kappa_o \left(1 - \left(\frac{Ri}{Ri_{cr}}\right)^2\right)^3 \tag{6}$$

for $Ri < Ri_{cr}$. We have chosen κ_o=1.8 $\times$ 10^{-4} m^{2}s^{-1} and Ri_{cr}=0.3, which gives a reasonable fit to data collected in the western equatorial Pacific [c.f. *Richards et al.*, 2015]. Both these values are well below those suggested by *Large et al.* [1994] (namely

50×10^{-4} m^2s^{-1} and 0.7, respectively). (A value of Ri_{cr}=0.3 gives a better fit to the data than Ri_{cr}=0.25 shown in Fig. 8 of *Richards et al.*, 2015, for values of Ri around 0.25.) The results are somewhat sensitive to the choice of Ri_{cr}. For instance the mean value between 150-250m is reduced by approximately 25% with Ri_{cr}=0.25, but increased by more than a factor of 3 for Ri_{cr}=0.7, for both time series. (Employing the value of κ_o suggested by *Large et al.* [1994] increases κ_{KPP} by a factor close to 30)

Despite the large vertical variations in $\tilde{u}$ and N, there are qualitative similarities between the profiles of κ_v and κ_{KPP}. There are, however, important quantitative differences. For instance above 125m depth there is an increase in κ_v at 1.375°N compared with the equator. With κ_{KPP} there is a decrease between the two. κ_{KPP} captures the local maximum in κ_v centered around 150m at both sites, but is smaller in magnitude and does not display the large increase at 1.375°N. Below 250m κ_{KPP} diverges from κ_v. As stated above, for κ_v, given by (5), the reduction with depth in $\tilde{u}$ below the thermocline (see Figs. 9a and 10a) partially compensates for the reduction in N. For KPP, with a constant κ_o, there is no compensation and the KPP estimate at 350m is approximately 3 times that given by (5) at both sites.

7. Discussion

We have presented a framework to study shear–generated turbulence and its scaling. We have couched the problem in terms of readily measured quantities in the ocean or atmosphere or easily derived quantities in models. A major assumption is that the Richardson number is an important parameter in determining whether or not there is turbulent activity. A key aspect, however, is to shift emphasis away from the functional form of the Richardson number to consideration of the time and length scales controlling the turbulent

activity. In particular, we assume a scaling for the vertical length scale of the turbulent flow found from theoretical considerations, DNS studies and previous measurements in the western equatorial Pacific.

To test our proposed scaling we have compared it to observations of the turbulent kinetic energy dissipation rate, ϵ, taken in the western equatorial Pacific. The time averaged ϵ estimated by the scaling given by (1) using the data from time series compares well with the observed average. The estimated ϵ captures the differences in observed vertical structure and amplitude of the two time series. Much of the vertical variation of ϵ is found to be controlled by the vertical variation in velocity scale, $\tilde{u}$, of the fine scale (small vertical scale) velocity variations (SVSs).

The western equatorial Pacific is an ideal location to study shear–generated turbulence. The vertical shear responsible for much of the turbulent activity often has a distinct vertical scale that is resolvable using appropriate instrumentation [*Richards et al.*, 2015]. Here we emphasize the need to resolve the appropriate flow structures when making direct comparisons of flow features, such as the vertical shear, and turbulence activity (as opposed to making assumptions about the spectral characteristics of the shear as in the approach of e.g. *Gregg*, 1989, and related studies).

An aspect that warrants further investigation is the turbulent velocity scale u_t. Here we have assumed it to be related to the velocity scale of the flow features that dominate the vertical shear, $\tilde{u}$. We average over a number of turbulent events at various times in their evolution during the $\sim$7 day time series. Based on DNS studies this is a not an unreasonable assumption [c.f. *Smyth et al.*, 2005], although those studies show the relationship to vary as a turbulent event evolves. There may be differences, therefore,

in a time–averaged sense for different flow regimes and appropriate DNS studies, as well as observations in different regimes, are required to determine those differences. In the present study the shear during the equatorial time series was very persistent in time (Fig. 2a) and most likely induced by inertial instability. Wind–generated inertia gravity waves can produce event-like mixing events [e.g. *Soares et al.*, 2016] which may have different time-averaged characteristics. We note, however, the shear at 1.375°N is less temporally coherent than at the equator, apart from along the pycnocline (Fig. 2c). Despite these differences our scaling for u_t appears to work well for both time series.

We find the vertical distribution of the estimated vertical diffusion coefficient is dependent on the vertical variations of Ri, $\tilde{u}$ and N. Indeed, if the variations in the latter two are ignored, such as in KPP, there are substantial differences in the vertical distribution (see Fig. 11). But how important is the vertical variation in the vertical diffusion coefficient? This needs to be ascertained for particular flows. *Sasaki et al.* [2013] find it to be important for large-scale ocean–atmosphere interactions in the tropical Pacific. In a related study *Jia et. al.* [2021], in press, find with enough vertical resolution in a model of the tropical Pacific (enough to start to resolve the observed fine scale structures in the vertical shear) the associated vertical distribution of the eddy diffusivity (derived using KPP) changes the structure of the equatorial thermocline, which in turn impacts the temperature in the equatorial Pacific cold tongue. It remains to be seen how large an impact the differences seen in Figure 11 have.

Acknowledgments. Data used in this study were collected on cruise KM1208 of the R/V Kilo Moana and can be found at the R2R data archive at

https://www.rvdata.us/search/vessel/km1208 & km1225 with microstructure data at https://microstructure.ucsd.edu/.

We are particularly thankful to Captain Dewry and crew of the R/V Kilo Moana and the UH OTG for their expertise and enthusiastic help in collecting the data. This work was supported by the U.S. National Science Foundation under grant NSF OCE-1029722. KJR also acknowledges support from the Kavli Institute of Theoretical Physics and the National Science Foundation under grant NSF PHY-1748958.

References

Bartello, P., and S. M. Tobias (2013), Sensitivity of stratified turbulence to the buoyancy Reynolds number, *J. Fluid Mech.*, *725*, 1–22.

Brethouwer, G., P. Billant, E. Lindborg, and J.-M. Chomaz (2007), Scaling analysis and simulation of strongly stratified turbulent flows, *J. Fluid Mech.*, *585*, 343–368.

Godeferd, F. S., and C. Staquet (2003), Statistical modelling and direct numerical simulations of decaying stably stratified turbulence. Part 2. Large–scale and small–scale anisotropy, *J. Fluid Mech.*, *486*, 115–159.

Gregg, M. (1989), Scaling turbulent dissipation in the thermocline, *J. Geophys. Res.*, *94*, 9686–9698.

Ijichi, T., and T. Hibiya (2018), Observational variations in turbulent mixing efficiency in the deep ocean, *Journal of Physical Oceanography*, *48*(8), 1815–1830, doi:10.1175/JPO-D-17-0275.1.

Koop, C. G., and F. K. Browand (1979), Instability and turbulence in a stratifed fluid with shear, *J. Fluid Mech.*, *93*, 135–159.

Kunze, E., A. J. Williams III, and M. G. Briscoe (1990), Observations of shear and verticalstability from a neutrally buoyant float, *J. Geophys. Res.*, *95*(C10), 18,127–18,142.

Large, W. G., J. C. McWilliams, and S. C. Doney (1994), Oceanic vertical mixing: a review and model with a nonlocal boundary layer parameterisation, *32*, 363–403.

Natarov, A., and K. J. Richards (2015), Persistent presence of small vertical scale velocity features during three–dimensional equilibration of equatorial inertial instability, *Physics of Fluids*, *27*, 84,109, doi:10.1063/1.49283199.

Osborn, T. R. (1982), Estimates of the local rate of vertical diffusion from dissipation measurements, *J. Phys. Oceanogr.*, *10*, 83–89.

Pacanowski, R., and S. Philander (1981), Parameterization of vertical mixing in mumerical models of tropical oceans, *J. Phys. Oceanogr.*, *11*, 1443–1451.

Peters, H., M. C. Gregg, and J. M. Toole (1988), On the parameterisation of equatorial turbulence, *J. Geophys. Res.*, *93*, 1199–1218.

Richards, K. J., and N. R. Edwards (2003), Lateral Mixing in the Equatorial Pacific: the importance of inertial instability, *Geophys. Res. Lett.*, *30*, 1888, doi:10.1029/2003GL017768.

Richards, K. J., A. Natarov, E. Firing, Y. Kashino, S. M. Soares, M. Ishizu, G. S. Carter, J. H. Lee, and K. I. Chang (2015), Shear-generated turbulence in the equatorial Pacific produced by small vertical scale flow features, *J. Geophys. Res.*, *120*, 3777–3791.

Sasaki, W., K. J. Richards, and J.-J. Luo (2013), Impact of vertical mixing induced by small vertical scale structures above and within the equatorial thermocline on the tropical Pacific in a CGCM, *Climate Dynamics*, *41*(2), 443–453, doi:10.1007/s00382-

012-1593-8.

Smyth, W. D., J. D. Nash, and J. N. Moum (2005), Differential diffusion in breaking Kelvin–Helmholtz billows, *J. Phys. Oceanogr.*, *35*, 1004–1022.

Soares, S. M., A. Natarov, and K. J. Richards (2016), Internal swells in the tropics: Near–inertial wave energy fluxes and dissipation during CINDY, *J. Geophys. Res.*, *121*, 3297–3324, doi:10.1002/2015JC01160.

Vallis, G. K. (2006), *Atmospheric and Oceanic Fluid Dynamics*, 745 pp., Cambridge University Press, Cambridge, U.K.

Waite, M. L., and P. Bartello (2004), Stratified turbulence dominated by vortical motions, *J. Fluid Mech.*, *517*, 281–308.

Zaron, E. D., and J. N. Moum (2009), A new look at Richardson number mixing schemes for equatorial ocean modeling, *J. Phys. Oceanogr.*, *39*, 2652–2664.

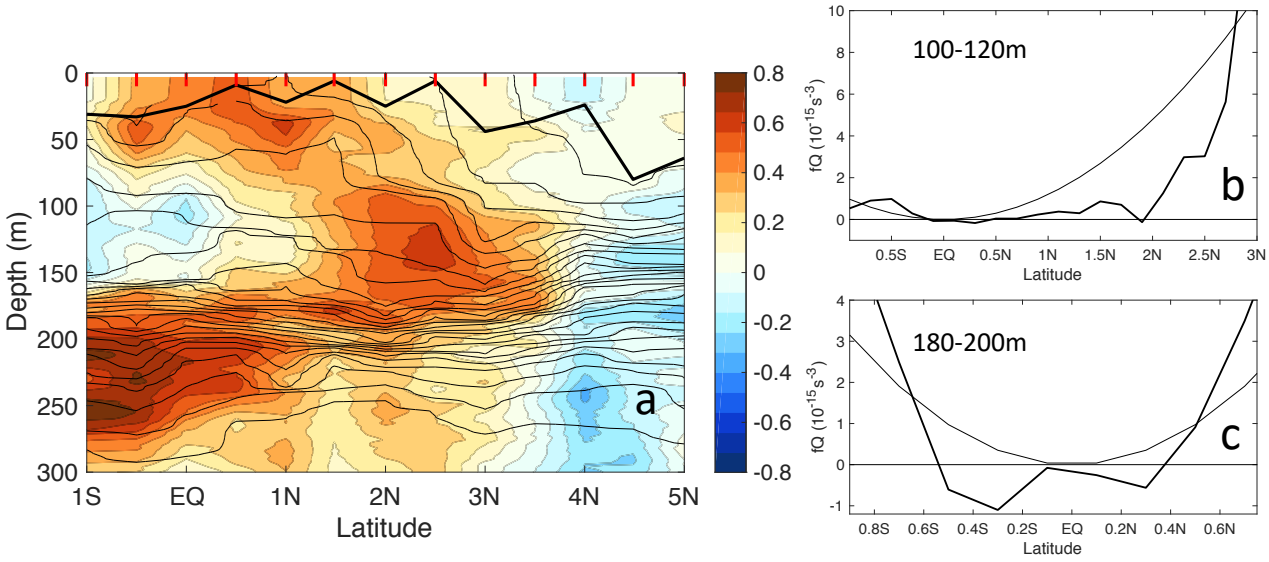

Figure 1. (a) The eastward (zonal) component of velocity, u, measured along 156°E in April 2012. Red colors indicate eastward flow, blue westward. Gray lines: contours of potential density (contour interval: 0.2 kgm^{-3}). Black line: mixed layer depth (b) fQ along isopycnals (see text for definition) averaged between isopycnals with mean depth 100-120m as a functional of latitude (c) Same as (b) but averaged between 180-200m. The thin lines in (b) and (c) are $f^2 N_0^2$, where N_0^2 is the average N^2 along the layers. (Note, the latitudinal ranges in (b) and (c) are different.)

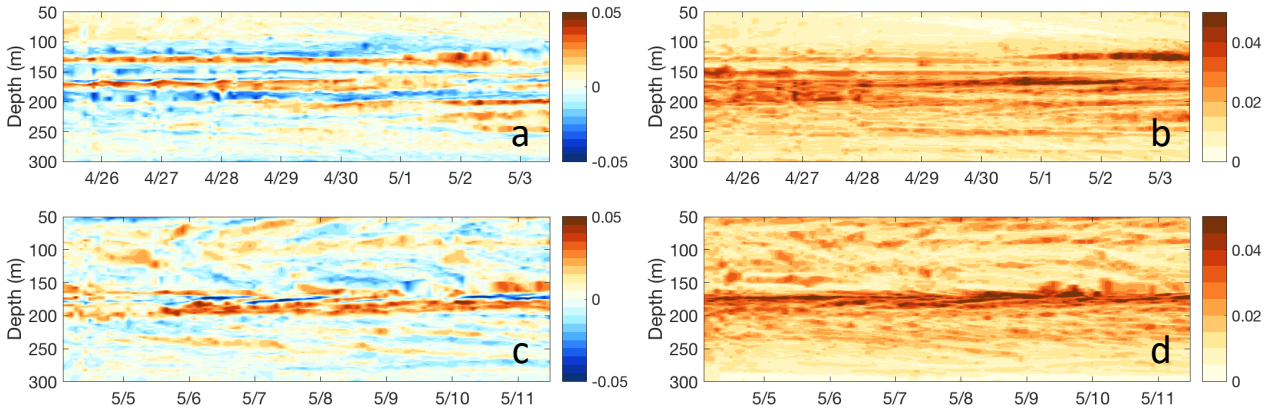

Figure 2. Time series of variables on potential density surfaces at the equator, 156°E plotted as mean depth of the density surface versus time: (a) vertical shear of the meridional component of velocity, $\partial v/\partial z$ (s^{-1}), (b) Buoyancy frequency, N (s^{-1}). (c) and (d): as (a) and (b) but for the time series at 1.375°N, 156°E. Time is given as month/day for the year 2012.

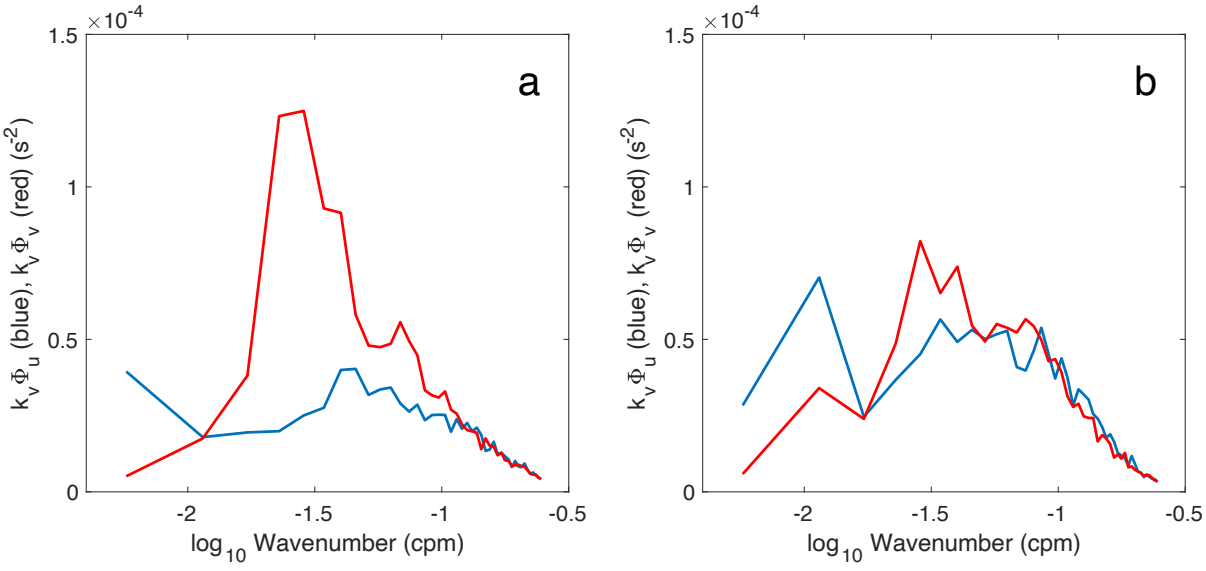

Figure 3. Variance preserving spectra of the zonal and meridional components of shear as a function of vertical wavenumber: (a) equator, 156°E (b) 1.375°N, 156°E.

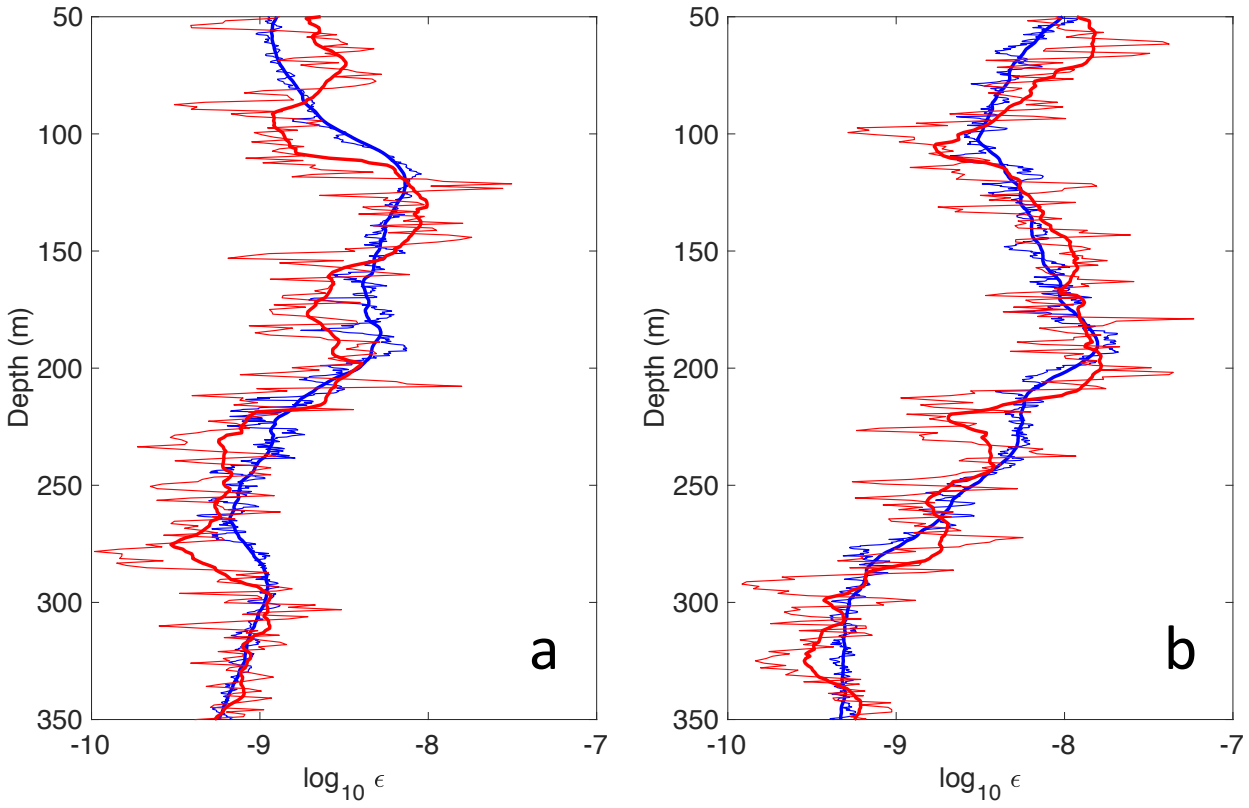

Figure 4. (a) Time mean turbulent kinetic energy dissipation rate, ϵ (Wkg^{-1}), for the time series at the equator, as a function of depth (thin lines). Thick lines: with 10m running averaged applied. Red lines: observed. Blue lines: estimated using (1), (2) and (3). (b) As (a) but for the time series at 1.375°N.

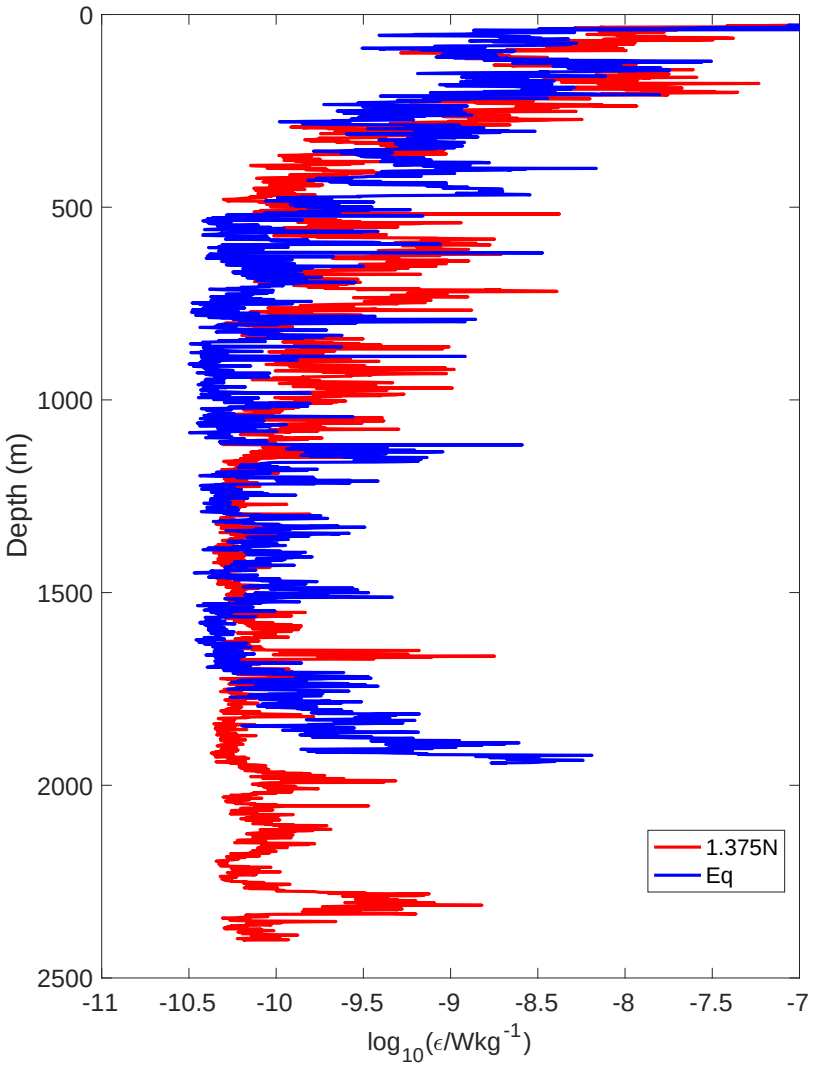

Figure 5. Time mean turbulent kinetic energy dissipation rate, ϵ (Wkg^{-1}), over the full depth of profiles for the time series at the equator (blue) and 1.375°N (red).

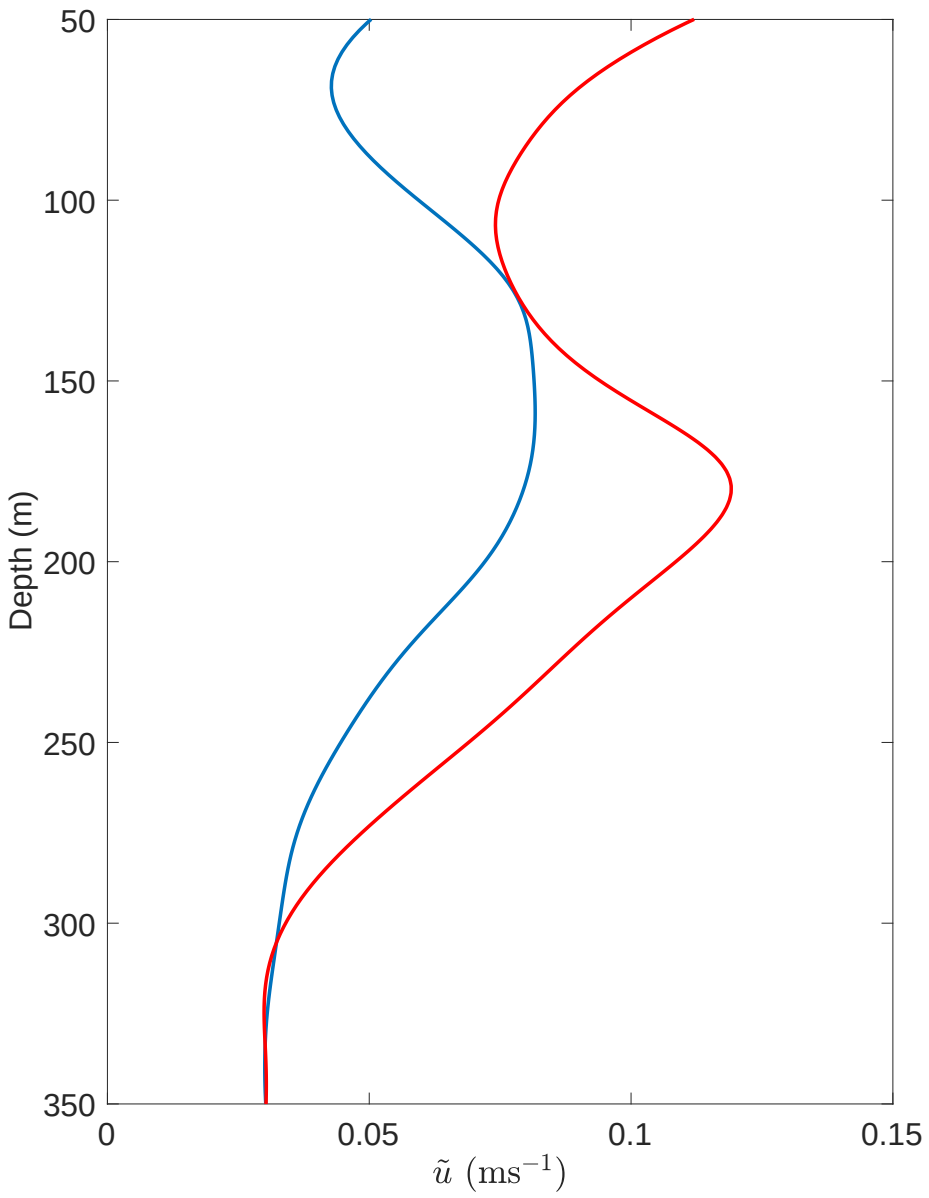

Figure 6. The time mean of the SVS velocity scale, $\tilde{u}$. as a function of depth (see text for definition). Blue line: equatorial time series. Red line: 1.375°N time series.

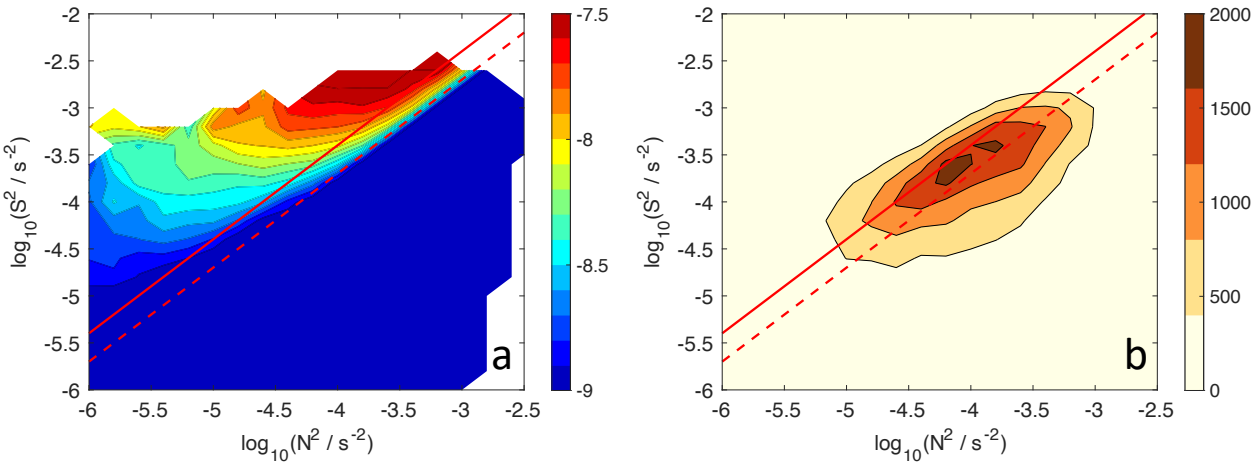

Figure 7. (a) Turbulent kinetic energy dissipation rate, ϵ, estimated from (1), bin averaged with respect to $\log_{10}S^2$ and $\log_{10}N^2$, for the equatorial time series for data between depths 50-250m. (b) Number of occurrences in each bin average. Solid red line Ri=0.25. Dashed red line Ri=0.5

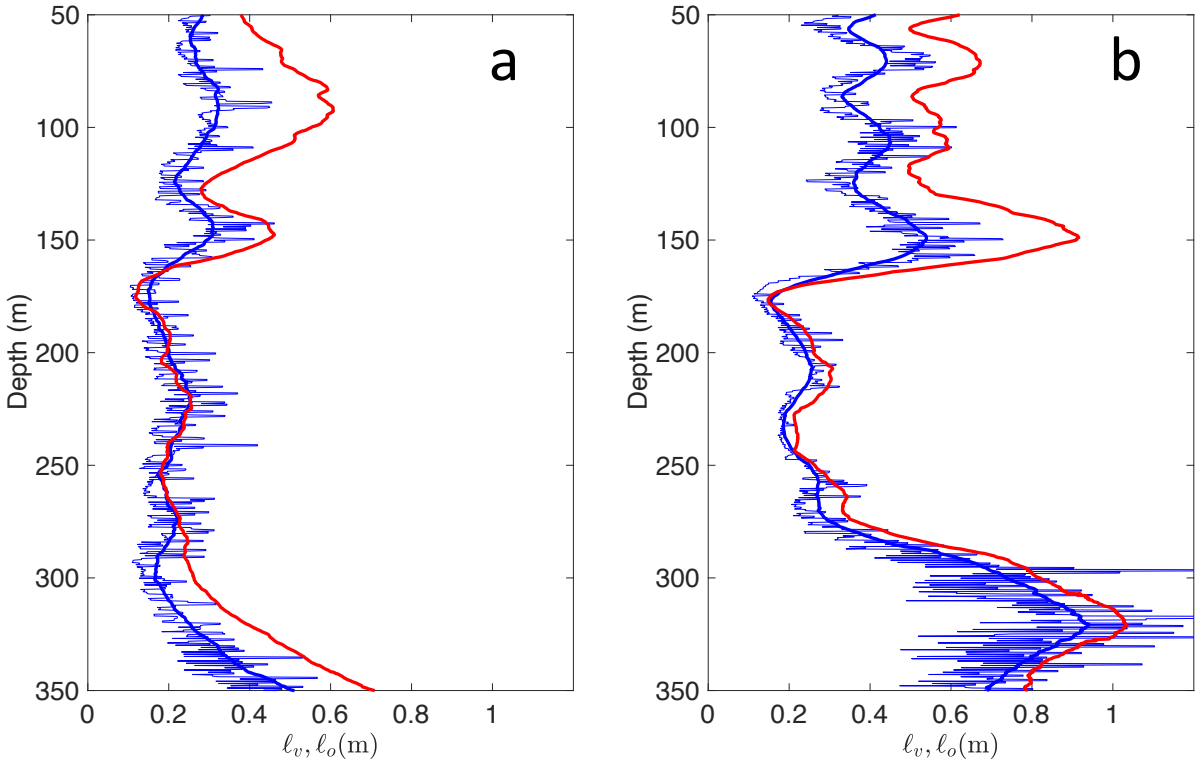

Figure 8. (a) Time mean of the turbulent length scale ℓ_v against depth (blue thin line), with a 10m running averaged applied (thick blue line) and the time mean of the Osmidov length scale ℓ_o with a 10m running averaged applied (thick red line), for the equatorial time series. (b) as (a) but for the 1.375°N time series.

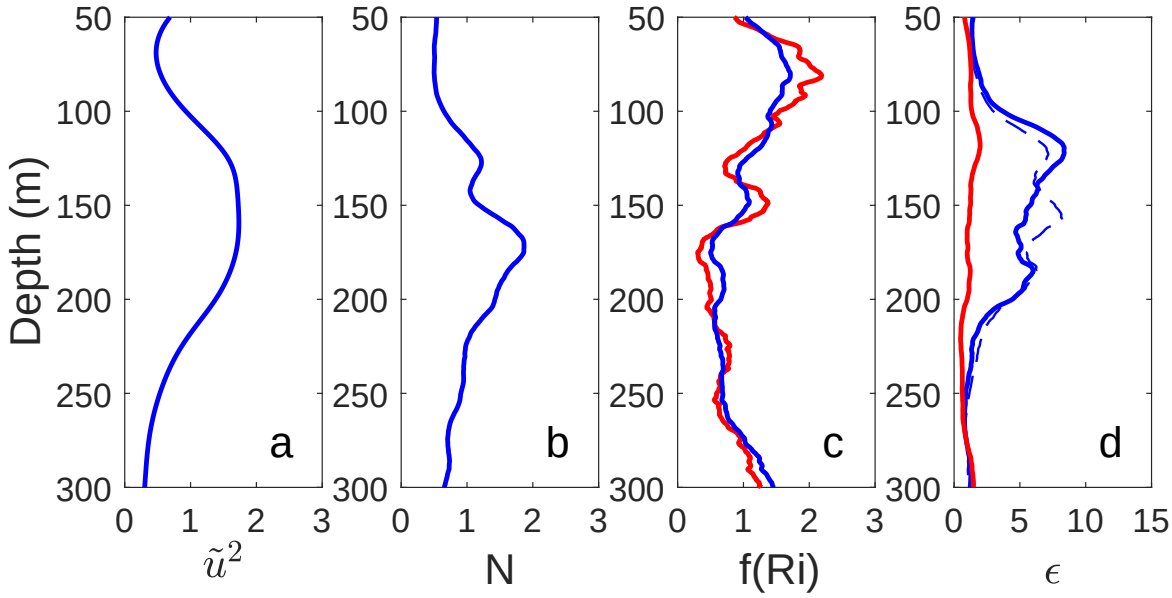

Figure 9. Normalized time mean of quantities from the equatorial time series. (a) $\tilde{u}^2$, (b) N and (c) f(Ri), normalized with their depth averages over the depth interval 50-300m. (d) estimated turbulent kinetic energy dissipation rate, ϵ, normalized with its value averaged between 250-300m. In (c): blue line $f(Ri)$ using (3), red line using $f_k(Ri)$ from *Kunze et al.* [1990]. In (d): blue line, ϵ estimated from (4); red line, ϵ estimated from $Nf(Ri)$; dashed blue line, product of the time mean of quanitities on the RHS of 1).

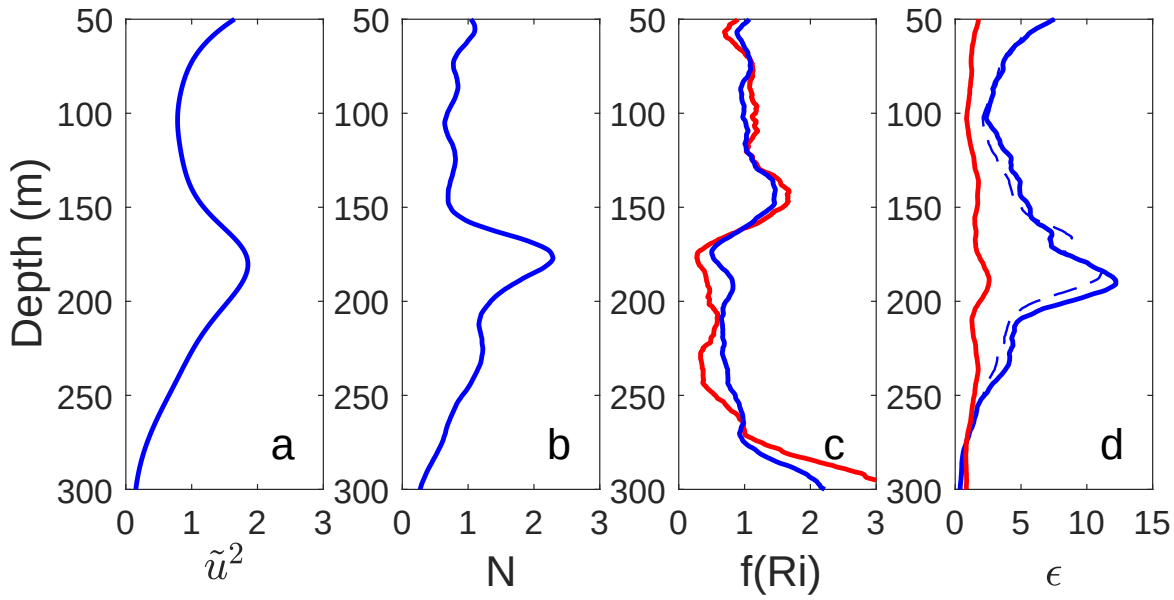

Figure 10. Same as Figure 9 except from the time series at 1.375°N

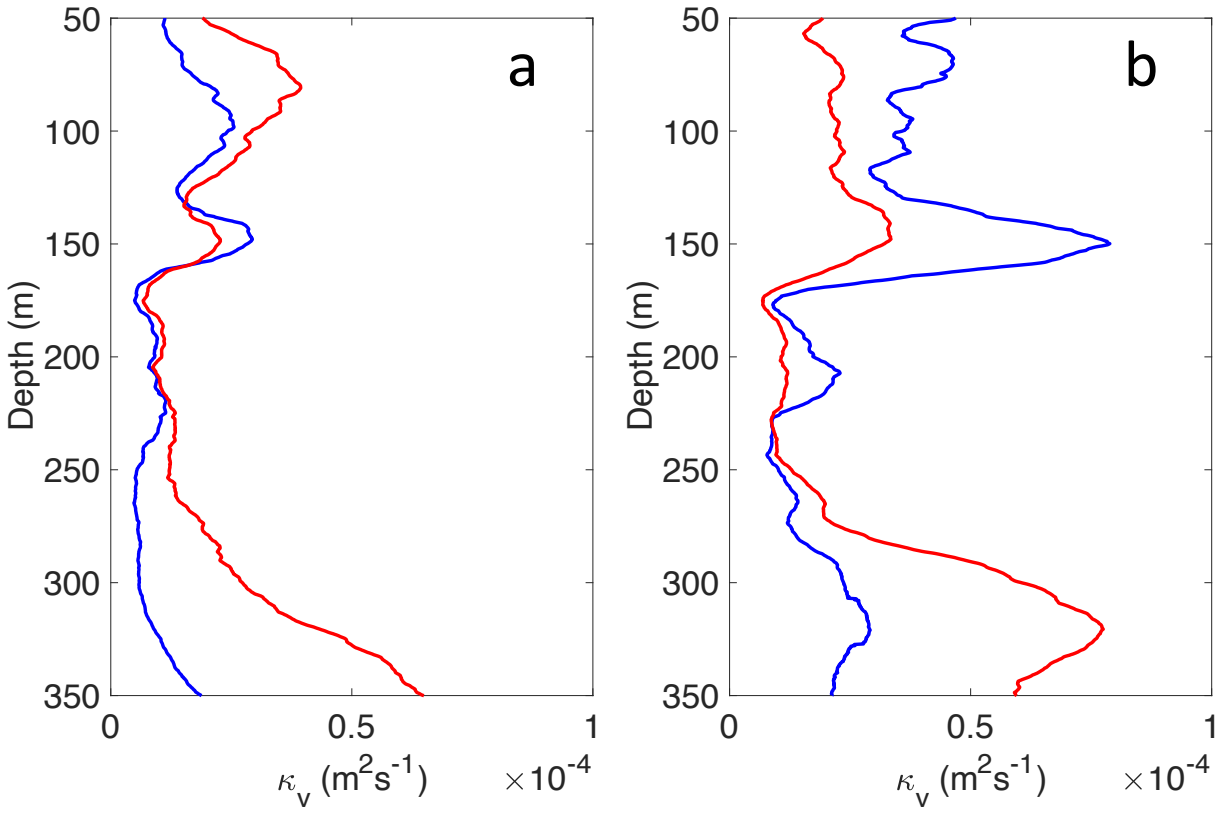

Figure 11. (a) Time mean vertical diffusion coefficient, κ_v. (a) at the equator. (b) at 1.375°N. Blue line: estimated by (5). Red line: KPP estimate (6) with κ_o=1.8 $\times$ 10^{-4} m^{2}s^{-1} and Ri_{cr}=0.3. A 10m running mean has been applied to each profile.